



Cite this: *Phys. Chem. Chem. Phys.*,  
2025, 27, 13991

# Molecular dynamics insights into tetrahydrofuran-assisted formation of CH<sub>4</sub>, CO<sub>2</sub>, and H<sub>2</sub> gas hydrates

Ramkhelavan Kanaujiya, <sup>a</sup> Atanu K. Metya, \*<sup>b</sup> Nilesh Choudhary, <sup>c</sup> Rajnish Kumar <sup>a</sup> and Tarak K Patra \*<sup>ad</sup>

Gas hydrates, also known as clathrate hydrates, are crystalline compounds formed when water molecules organize into cage-like structures that encapsulate gas molecules under conditions of high pressure and low temperature. These hydrates occur naturally in permafrost regions and deep-sea sediments and have gained significant interest as potential energy sources and for applications in gas storage, transportation, and sequestration. Here, we deploy molecular dynamics (MD) simulations to investigate the molecular-level mechanisms governing the formation and stabilization of CH<sub>4</sub>, CO<sub>2</sub>, and H<sub>2</sub> hydrates in the presence of tetrahydrofuran (THF). We analyze key structural and energetic properties, including tetrahedral order parameters, cage dynamics, and gas uptake throughout different hydrate formation stages: pre-nucleation, nucleation (induction), growth, and saturation. Our findings provide insights into the role of THF concentration in altering hydrate phase behavior, as well as kinetic and gas occupancy preferences within hydrate cages. The study offers a comprehensive understanding of hydrate nucleation mechanisms and thermodynamic stability, contributing to advancements in gas hydrate applications for energy and environmental technologies.

Received 25th April 2025,  
Accepted 13th June 2025

DOI: 10.1039/d5cp01574j

rsc.li/pccp

## 1. Introduction

Gas hydrates, also known as clathrate hydrates, are solid crystalline compounds in which water molecules, bonded through hydrogen bonds, form polyhedral cages that encapsulate various gas molecules such as carbon dioxide (CO<sub>2</sub>), methane (CH<sub>4</sub>), hydrogen (H<sub>2</sub>), nitrogen (N<sub>2</sub>), hydrogen sulfide (H<sub>2</sub>S), ethane, propane, and butane under high-pressure and low-temperature conditions.<sup>1–4</sup> Substantial deposits of gas hydrates are naturally found in permafrost regions and deep-sea sediments, which has led to significant interest in their potential as major energy sources.<sup>5,6</sup> Meanwhile, clathrate hydrate-based technologies are increasingly being employed in diverse, innovative applications, including the separation, storage, transportation, and sequestration of natural gases and greenhouse gases, wastewater treatment and desalination, oil, and gas flow assurance due to their

complete recovery of environmental friendliness, and non-explosive nature, which make them particularly attractive.<sup>7,8</sup>

In general, there are three widely recognized hydrate crystalline structures (see Scheme 1): structure I (sI), structure II (sII), and structure H (sH).<sup>9,10</sup> These structures are made by various combinations of cages, including the pentagonal dodecahedron, tetrakaidecahedron, hexakaidecahedron, pentagonal irregular dodecahedron, and icosahedron.<sup>11–13</sup> The formation of these structures seems strongly depend on the size and shape of the guest molecules involved, as well as the conditions present during gas hydrate formation.<sup>14</sup> Furthermore, in our earlier studies, we have shown that the composition of a gas mixture dictates the crystallinity of the gas hydrate structures.<sup>15</sup>

Several strategies have been employed to promote hydrate nucleation and enhance gas content in clathrate hydrates, including stirring or mixing, reactor design, and the addition of additives.<sup>16,17</sup> Different types of promoters have diverse impacts on hydrate formation and are typically classified as kinetic and thermodynamic promoters.<sup>18</sup> Kinetic promoters, such as surfactants, polymers, amino acids, and nanofluids, improve the kinetics of hydrate formation by increasing the solubility of the gas in the solution, thereby accelerating the formation rate.<sup>19,20</sup> For example, sodium dodecyl sulfate (SDS) surfactant molecule has displayed a remarkable impact on the rate of formation of the gas hydrates.<sup>21</sup> On the other hand, thermodynamic promoters

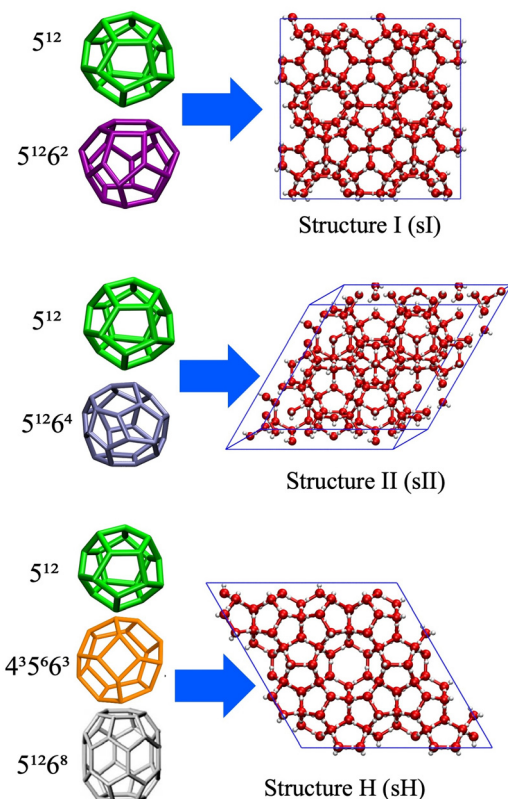
<sup>a</sup> Department of Chemical Engineering, Indian Institute of Technology Madras, Chennai, Tamil Nadu – 600036, India. E-mail: tpatra@iitm.ac.in

<sup>b</sup> Department of Chemical and Biochemical Engineering, Indian Institute of Technology Patna, Patna – 801106, India. E-mail: atanu.metya@iitp.ac.in

<sup>c</sup> Department of Chemical Engineering, Indian Institute of Technology Tirupati, Tirupati, Andhra Pradesh – 517619, India

<sup>d</sup> Center for Atomistic Modeling and Materials Design, Indian Institute of Technology Madras, Chennai, TN-600036, India





Scheme 1 Schematic representation of different clathrate hydrate structures and their constituent building cages.

modulate the hydrate equilibrium conditions to more favorable reaction conditions (*i.e.*, lower pressure and higher temperature) by increasing gas–liquid contact and stabilizing the hydrate cage structure through their presence in the cavity.<sup>22</sup> Several thermodynamic promoters, including tetrahydrofuran (THF), cyclopentane (CP), methylcyclohexane (MCH), neohexane, tetrabutylammonium chloride (TBAC), tetra-*n*-butylammonium chloride (TBAC), and tetrabutylammonium bromide (TBAB), have been identified and examined for their effects on gas hydrate formation.<sup>19,20</sup> Especially it is well known from previous studies that tetrahydrofuran (THF), which forms an sII type of hydrate structure, is an excellent thermodynamic promoter that significantly affects gas hydrate nucleation and growth by moderating equilibrium conditions, reducing nucleation induction time, and enhancing the formation rate.<sup>23,24</sup>

Lee *et al.*<sup>25</sup> investigated the phase equilibrium behavior of gas hydrates in the presence of THF and found that the dissociation conditions of the hydrates shifted to higher temperatures and lower pressures than those of pure hydrates. Additionally, they observed that the dissociation conditions of CH<sub>4</sub> and CO<sub>2</sub> gas hydrates depend on the THF concentration, identifying an optimal stoichiometric concentration of 5.56 mol% THF in the aqueous solution. Wang *et al.* investigated the effect of THF and THF/SDS on CO<sub>2</sub> hydrate formation and reported that THF significantly reduces the induction time. Furthermore, the combined use of THF and SDS enhances the gas storage density compared to systems containing only THF or no

additives.<sup>26</sup> Phan *et al.* recently studied the effect of THF on the kinetics of CO<sub>2</sub> hydrate growth and dissociation using molecular dynamics and demonstrating that THF facilitates CO<sub>2</sub> diffusion and shifts the favorable conditions for hydrate formation and stability to lower pressures and higher temperatures compared to systems without THF.<sup>27</sup>

Kumar *et al.*<sup>28</sup> demonstrated a two-step hydrate formation mechanism in a 5.56 mol% THF solution and elucidated the synergistic effect between CH<sub>4</sub> and THF in forming mixed CH<sub>4</sub>–THF hydrates. Recently, Ge *et al.*<sup>29</sup> reported that CH<sub>4</sub> gas molecules occupy the small cavities of the sII hydrate structure, with their occupancy increasing with the THF concentration, while THF molecules preferentially enter the large cavities, as determined through *in situ* Raman spectroscopy measurements. Furthermore, they found that CH<sub>4</sub> and CH<sub>4</sub>–THF hydrates coexist at 2.78 and 4.17 mol% THF, with gas consumption being 2.2 times greater compared to hydrate formation at 5.56 mol% THF. Strobel *et al.*<sup>30</sup> developed a thermodynamics model to capture the phase behavior of various gas hydrates in the presence of THF and provide insights into hydrogen filling in hydrate cavities, which largely depend on the pressure. Khurana *et al.* proposed a mass transfer-based model for the CH<sub>4</sub>–THF system, where methane diffuses through a THF hydrate layer and becomes encapsulated in hydrate cages.<sup>31</sup> Jiyang *et al.* demonstrated that CH<sub>4</sub>–THF hydrates can form under milder conditions, enabling efficient gas storage.<sup>32</sup> Mahant *et al.* reported the first measurements of CH<sub>4</sub>–THF hydrate nucleation rates and formation probability using a high-pressure automated reactor, providing valuable insights into phase equilibria and nucleation behavior.<sup>33</sup>

Hashimoto *et al.*<sup>34</sup> studied the phase equilibrium of mixed H<sub>2</sub>–THF hydrate systems with varying THF concentrations and found the three-phase line shifted to lower pressure or higher temperature compared to pure stoichiometric THF solutions. Zhang *et al.* reported that THF effectively promotes H<sub>2</sub> clathrate hydrate formation under milder conditions, with optimal concentrations enhancing formation kinetics, making it a promising route for safe and efficient hydrogen storage.<sup>35</sup> Experimental studies using high-pressure differential scanning calorimetry have explored the formation and dissociation of H<sub>2</sub> hydrates in the presence of THF, emphasizing the crucial influence of operating pressure on hydrate stability.<sup>36–38</sup> Although several studies have investigated the kinetics of CO<sub>2</sub> and CH<sub>4</sub> hydrate formation and a few experimental studies have explored H<sub>2</sub> hydrates in the presence of THF, a systematic investigation examining the effect of increasing THF concentration (from 0 to 5.56 mol%) and comparing different gas hydrates remains lacking.

In our recent studies, we report how surfactants control the CH<sub>4</sub> hydrate growth,<sup>39</sup> The impact of additives on the growth of binary mixture gas hydrates.<sup>40</sup> Here, we ask the question whether the hydrate growth depends on the characteristics of gas molecules. Towards this end, we examine the molecular dynamics of hydrate growth for three gas molecules, *viz.*, CH<sub>4</sub>, CO<sub>2</sub>, and H<sub>2</sub> independently. Further, we study how these growth profiles of single-component gas hydrates are impacted by the presence of a thermodynamic promoter such as THF. The key molecular mechanisms for hydrate nucleation and growth are based on

water–gas coordinated structuring (tetrahedral order parameter, cage dynamics, and number of gas molecules in the hydrate region). The examined system properties are given the entire spectrum from pre-nucleation stage, nucleation (induction), growth, and saturation, as well as how properties are influenced by types of gas and varying amounts of THF. The  $\text{CH}_4$  hydrate is found to grow faster than the  $\text{CO}_2$  hydrate at the same thermodynamic conditions. However, the  $\text{H}_2$  hydrate growth is extremely slow compared to  $\text{CH}_4$  and  $\text{CO}_2$  hydrate cases under quiescent conditions. These guest molecule-dependent hydrate growth profiles seem to overlap in the presence of a small amount of THF. The work provides molecular mechanisms of hydrate growth and how it is impacted by the presence of a thermodynamic promoter *viz.*, THF.

## 2. Simulation model and methodology

Water is modelled using the TIP4P/ice force field.<sup>41</sup> We employ the EPM2<sup>42</sup> to model  $\text{CO}_2$ , and the OPLS-AA force field is used for methane<sup>43</sup> and hydrogen.<sup>44</sup> The AMBER<sup>45</sup> forcefield is used THF. The Lennard-Jones interaction between the cross-species is determined using the geometric mean combination rule. Each system contains 384 gas molecules and 2944 water molecules. The number of THF molecules in the systems is 0, 30, 48, 114, and 196, corresponding to 0, 0.90, 1.42, 3.40, and 5.56 mol% of THF in the solutions, respectively. The initial systems are prepared by randomly inserting molecules into a cubic box with dimensions of  $5 \times 5 \times 5 \text{ nm}^3$ , as shown in Fig. 1.

Water molecules are treated as rigid, and the LINCS algorithm<sup>46</sup> was used to maintain their rigid geometry. The short-range non-bonded interactions (van der Waals and Coulombic interactions) were truncated at 1.2 nm. The long-range electrostatic interactions were computed using the particle mesh Ewald (PME) summation method with a grid spacing of 0.1 nm and 1.2 nm real-space cutoff.<sup>47</sup> Periodic boundary conditions were applied in all three directions. The leapfrog integration scheme<sup>48</sup> with a time step of 2 fs was used to solve the equations of motion. The systems were initially energy-minimized using the

steepest descent method.<sup>49</sup> After that, it was subjected to an equilibration run in an isothermal-isobaric ensemble (NPT) for 5 ns at 300 K and 10 MPa. In the NVT equilibration, the temperature was controlled using the Berendsen thermostat<sup>50</sup> with a relaxation time of 0.2 ps. In the NPT equilibration, temperature was controlled using the Nose–Hoover thermostat<sup>51,52</sup> with a relaxation time of 0.5 ps, and pressure was controlled using the Parrinello–Rahman barostat<sup>53</sup> with a relaxation time of 2 ps. Finally, the gas hydrate simulations were carried out at 240 K and 50 MPa for 1 microsecond using the NPT ensemble. All simulations were conducted using GROMACS v.2023.<sup>54</sup> All the properties are averaged over three independent simulations

The order parameter,  $F_4$  is calculated to quantify the hydrate formation for all the cases. The  $F_4$  is defined as<sup>55</sup>

$$F_4 = \frac{1}{k} \sum \cos 3\varphi_i.$$

where,  $\varphi_i$  is the H–O–O–H torsional angle and  $k$  is the number of oxygen–oxygen pairs within 0.35 nm of the selected molecule. The  $F_4$  parameter was computed for the entire trajectory of production runs.

## 3. Results and discussion

All the systems are equilibrated in an isothermal-isobaric ensemble at 300 K and 10 MPa for 5 ns. These pre-nucleation simulations generate gas nanobubbles in water, as shown in Fig. 2. The shape of the bubbles appears to be spherical for  $\text{CH}_4$  and  $\text{CO}_2$ , however, it is cylindrical for  $\text{H}_2$ . This is due to the inherent lower density of  $\text{H}_2$ , which corresponds to the higher volume fraction when they aggregate in the simulation box. The gas molecule pair correlation function suggests that the correlation is strongest for  $\text{CH}_4$ ,  $\text{CO}_2$ , and  $\text{H}_2$  correlations are of similar strength. The correlation does not change significantly in the presence of THF. Prior works reported that methane forms a quasi-spherical bubble during methane hydrate dissociation, which then transforms into a cylindrical-shaped nanobubble due to the effect of interfacial tension.<sup>56</sup> Furthermore, the formation of spherical and cylindrical nanobubbles has been observed in an aqueous solution of  $\text{CH}_4/\text{CO}_2$  mixed gases during the initial simulation at a temperature of 300 K and a pressure of 10 MPa.<sup>57</sup> Recently, experimental measurements and simulation studies have confirmed the coexistence of  $\text{CO}_2$  nanobubbles and droplets during gas–hydrate dissociation.<sup>58</sup> Our results confirm the formation of nanobubbles during pre-equilibration. These gas–water two – phase systems obtained after pre-equilibration at 300 K and 10 MPa are then quenched to 240 K and 50 MPa. Under these conditions, simulations are run for 1000 ns, during which hydrates nucleate, grow, and reach a saturation.

We compare the  $F_4$  order parameter at various THF concentrations to assess its influence on the formation of gas hydrates. The  $F_4$  value is known to be around  $-0.04$  for liquid water,  $-0.4$  for ice, and approximately  $0.7$  for hydrate structure.<sup>55</sup> These distinct values allow for the differentiation between the aqueous and hydrate phases.

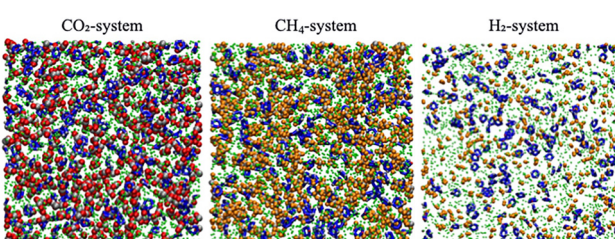


Fig. 1 The initial configurations of the gas–water mixtures in the presence of THF molecules. Each system contains 2944 water molecules and 196 THF (*i.e.*, 5.56 mol%). The left, middle, and right panels correspond to  $\text{CO}_2$ ,  $\text{CH}_4$ , and  $\text{H}_2$  gas systems, respectively. Small green spheres represent the oxygen atoms of water molecules. The carbon and oxygen atoms of  $\text{CO}_2$  molecules are depicted as grey and red large spheres, respectively. Orange spheres represent the hydrogen atoms of  $\text{CH}_4$  and  $\text{H}_2$  molecules, while grey spheres denote the carbon atoms of  $\text{CH}_4$ . THF molecules are represented by blue sticks. For clarity, the hydrogen atoms of both water and THF molecules are not shown.



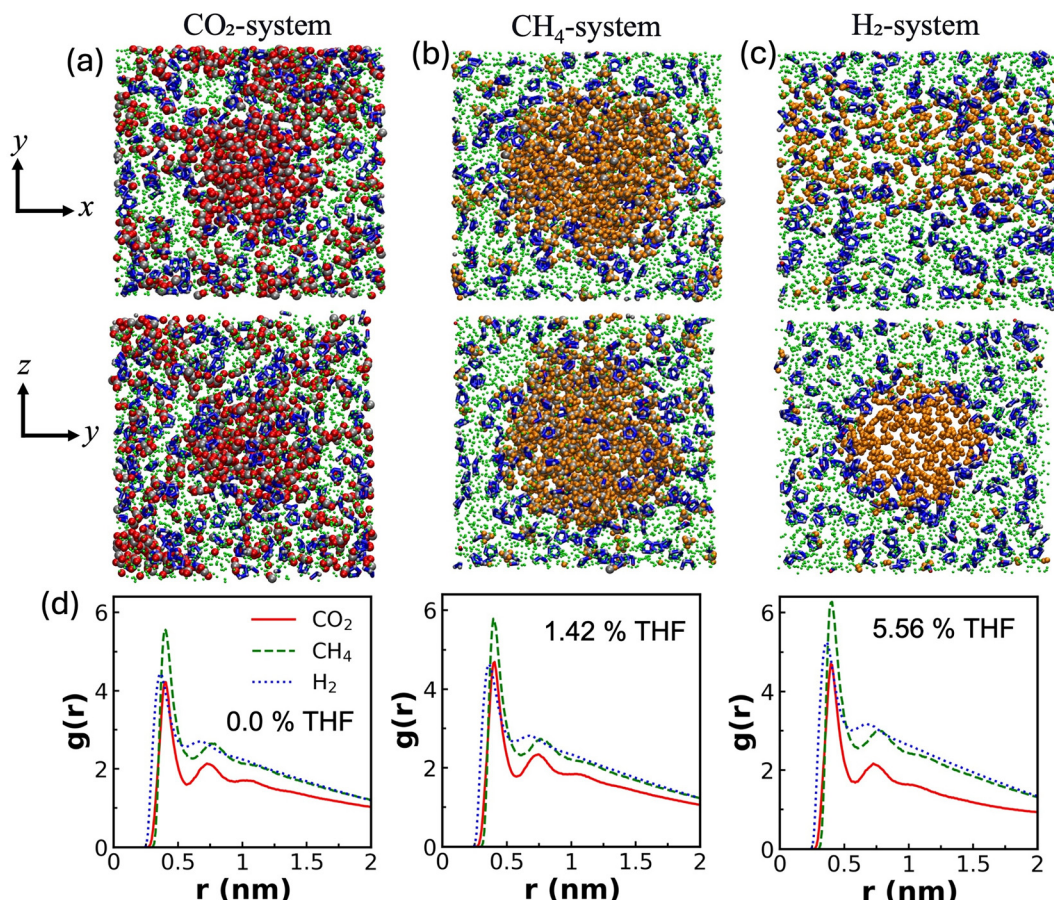


Fig. 2 Side views of MD snapshots captured at the end of 5 ns of initial equilibration at 300 K and 10 MPa in the presence of 5.56 mol% THF for gas systems: (a) CO<sub>2</sub>, (b) CH<sub>4</sub>, and (c) H<sub>2</sub>. Atom colors are the same as those denoted in Fig. 1. Panel (d) shows the radial distribution function of gas molecules computed over the 5–10 ns interval at 300 K and 10 MPa for THF concentrations of 0 (left), 1.42 (middle), and 5.56% (right).

Fig. 3a shows representative snapshots of the nucleation and growth processes during the simulation at THF concentrations of 0.9% and 5.56%, comparing systems containing different gases. During the nucleation phase, relatively stable clusters of 5<sup>12</sup> cages form, which subsequently promote the development and expansion of additional hydrate cages in the growth stage. Additionally, small gas molecules are initially encapsulated within the 5<sup>12</sup> cages in the early stages of hydrate formation. As hydrate nucleation begins, the  $F_4$  parameter increases (see Fig. 3), reflecting the progressive ordering of water molecules around guest species. In the early stages, water forms transient, hydrate-like structures around gas molecules (CO<sub>2</sub>, CH<sub>4</sub>, or H<sub>2</sub>), occasionally giving rise to short-lived 5<sup>12</sup> and 5<sup>12</sup>6<sup>2</sup> cages. These intermediate structures contribute to an increase in the  $F_4$  value from its baseline (−0.04 for liquid water), even though the number of fully formed hydrate cages remains limited due to repeated formation and dissociation. After a sufficient induction period, a stable number of cages form, marking the onset of nucleation. The corresponding  $F_4$  value at this point is dependent on the size and compactness of the nucleus. Typically,  $F_4$  values range between 0.1 and 0.2 during this transition. The shift from nucleation to growth is defined by the formation of a critical nucleus – a stable cluster of hydrate cages that can grow further. Following

nucleation, the system enters the growth phase, during which the size of the hydrate cluster increases, and the structure becomes more stable. This leads to a continued rise in the  $F_4$  parameter until it eventually plateaus, indicating the saturation of hydrate growth within the simulation timeframe.

Fig. 3b illustrates the  $F_4$  order parameter for THF concentrations of 0%, 0.9%, 1.42%, 3.4%, and 5.56% in the solutions. In the absence of THF, the  $F_4$  order parameter gradually increases with time for CO<sub>2</sub> gas and CH<sub>4</sub> gas, suggesting the gas hydrate formation, whereas the  $F_4$  value remains below 0.05 for the H<sub>2</sub> system, suggesting no hydrate formation within the nucleation timeframe. Even after extending the H<sub>2</sub>-water system simulation to 2  $\mu$ s, no nucleation was observed. At the pre-nucleation stage, the  $F_4$  value for CO<sub>2</sub> is slightly higher than that for CH<sub>4</sub>, indicating early ordering; however, as time progresses, the  $F_4$  value for CH<sub>4</sub> eventually surpasses that of CO<sub>2</sub>, reflecting a faster transition into the growth phase. We find that the  $F_4$  values are higher in the presence of THF compared to its absence, indicating that THF promotes faster gas hydrate formation. This finding is consistent with previous studies reporting that THF enhances the kinetics of gas hydrate formation.<sup>59–61</sup>

At low THF concentrations (0.9 and 1.42 mol%), the  $F_4$  values for the CH<sub>4</sub>-water and H<sub>2</sub>-water systems show minimal



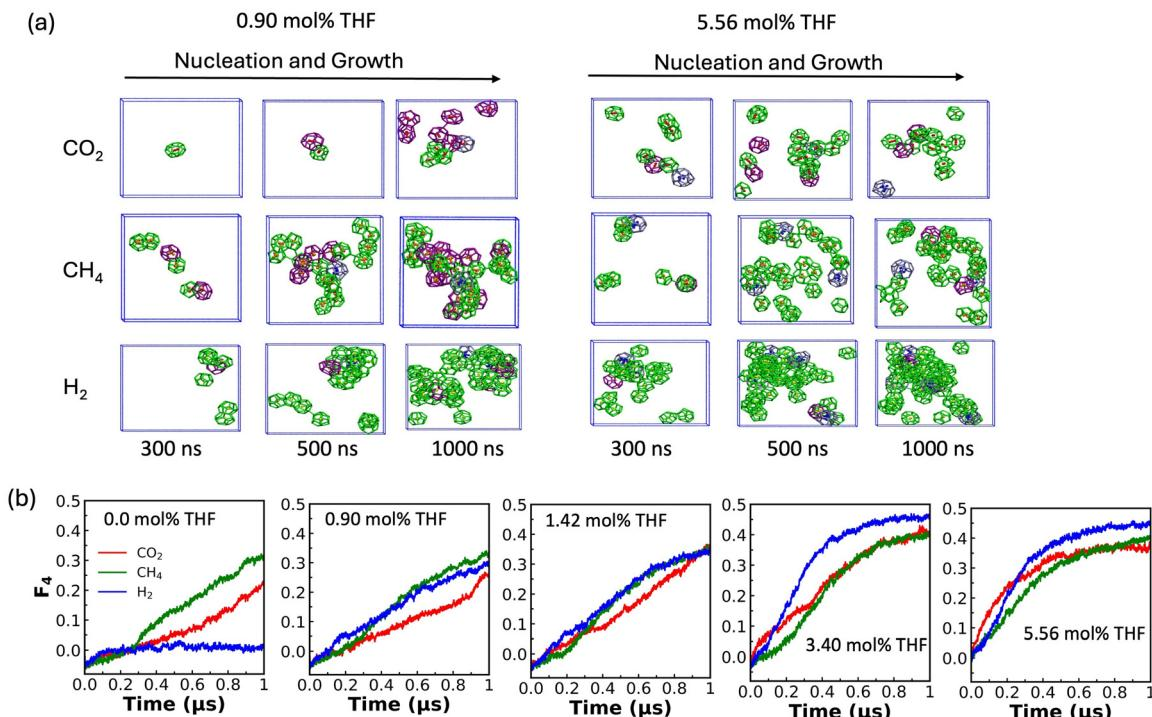


Fig. 3 (a) Snapshots illustrate the nucleation and growth process of gas hydrate formation with 0.9 mol% (left panel) and 5.56 mol% (right panel) THF in solution. Water molecules in the 5<sup>12</sup>, 6<sup>2</sup>5<sup>12</sup>, and 6<sup>4</sup>5<sup>12</sup> cages are connected by green, purple, and ice blue lines, respectively. (b) Evaluation of  $F_4$  order parameter is plotted as a function of time for three gas hydrates H<sub>2</sub> (blue), CH<sub>4</sub> (green), and CO<sub>2</sub> (red) with THF concentration of 0, 0.9, 1.42, 3.4, and 5.56 mol% in the solution, respectively.

variation, suggesting that the impact of THF on gas hydrate formation is less pronounced at lower concentrations. In contrast, at higher concentrations of THF, a significant difference in the  $F_4$  values is observed across the gas systems. As shown in Fig. 3, during the nucleation stage of gas hydrate formation, the  $F_4$  parameter trends as follows: CO<sub>2</sub> > H<sub>2</sub> > CH<sub>4</sub>, indicating that CO<sub>2</sub> hydrates nucleate earlier than H<sub>2</sub>, while CH<sub>4</sub> hydrates exhibit the slowest nucleation among the three gases. Nevertheless, the greater  $F_4$  value for H<sub>2</sub> at the end of the simulation period suggests a higher growth rate of H<sub>2</sub> hydrate formation compared to CO<sub>2</sub> and CH<sub>4</sub> gas hydrates. Thus, these results suggest that THF strongly affects gas hydrate nucleation and growth processes when its concentration exceeds 1.42%.

Next, we analyze cages that are formed in our simulations. The three most abundant cages in clathrate hydrate structures are identified through the connectivity of five- and six-membered rings formed by the first-neighbor water molecules, considering the atomic coordinates of the oxygen atoms in water. In this study, we employ the GRADE code developed by Mahmoodinbar and Dias<sup>62</sup> to identify three main types of cages: 5<sup>12</sup>, 5<sup>12</sup>6<sup>2</sup>, and 5<sup>12</sup>6<sup>4</sup>, which consist of 20, 24, and 28 water molecules, respectively. Fig. 4 illustrates the variation in the number of different types of cages over simulation time during the formation of CO<sub>2</sub>, CH<sub>4</sub>, and H<sub>2</sub> gas hydrates, both in the presence and absence of the THF in the solutions. The results indicate that hydrate-like ordering of water molecules first forms small 5<sup>12</sup> cages, which initiate gas hydrate formation

during the nucleation stage of all gas hydrates, while a few large 5<sup>12</sup>6<sup>2</sup> and 5<sup>12</sup>6<sup>4</sup> cages are formed during the growth process.

We find that a greater number of small 5<sup>12</sup> cages are formed compared to large 5<sup>12</sup>6<sup>2</sup> and 5<sup>12</sup>6<sup>4</sup> cages, and the total number of cages increases as the concentration of the promoter THF in the solution increases, indicating a strong influence of THF concentration on gas hydrate formation. Interestingly, the number of 5<sup>12</sup>6<sup>2</sup> cages increases as the THF concentration rises to 1.42% for CO<sub>2</sub> gas hydrate, while for CH<sub>4</sub> gas hydrate, the number of 5<sup>12</sup>6<sup>2</sup> cages decreases with increasing THF concentrations. On the other hand, there is an insignificant effect of THF concentration on the formation of large cages for H<sub>2</sub> gas hydrate. At 0% THF concentration, 1–3 small 5<sup>12</sup> cages form during prenucleation, however, there is no H<sub>2</sub> clathrate formation within the 1 ns simulation time. Fig. 5 shows the total average number of cage (5<sup>12</sup>, 5<sup>12</sup>6<sup>2</sup>, and 5<sup>12</sup>6<sup>4</sup>) formations with varying THF concentrations in the solutions for the last 100 ns of the simulations. We find that the total number of cages increases with increasing THF concentration up to 3.4%. However, beyond this concentration, there is a noticeable decline in cage formation. Furthermore, within the 0.9–3.4% THF concentration, the number of cages formed in CH<sub>4</sub> and H<sub>2</sub> gas hydrates is approximately twice that observed in CO<sub>2</sub> gas hydrate. These findings indicate that THF has a strong influence on gas hydrate formation and that the extent of cage formation is strongly dependent on THF concentration. Moreover, the variations in cage structures suggest the potential

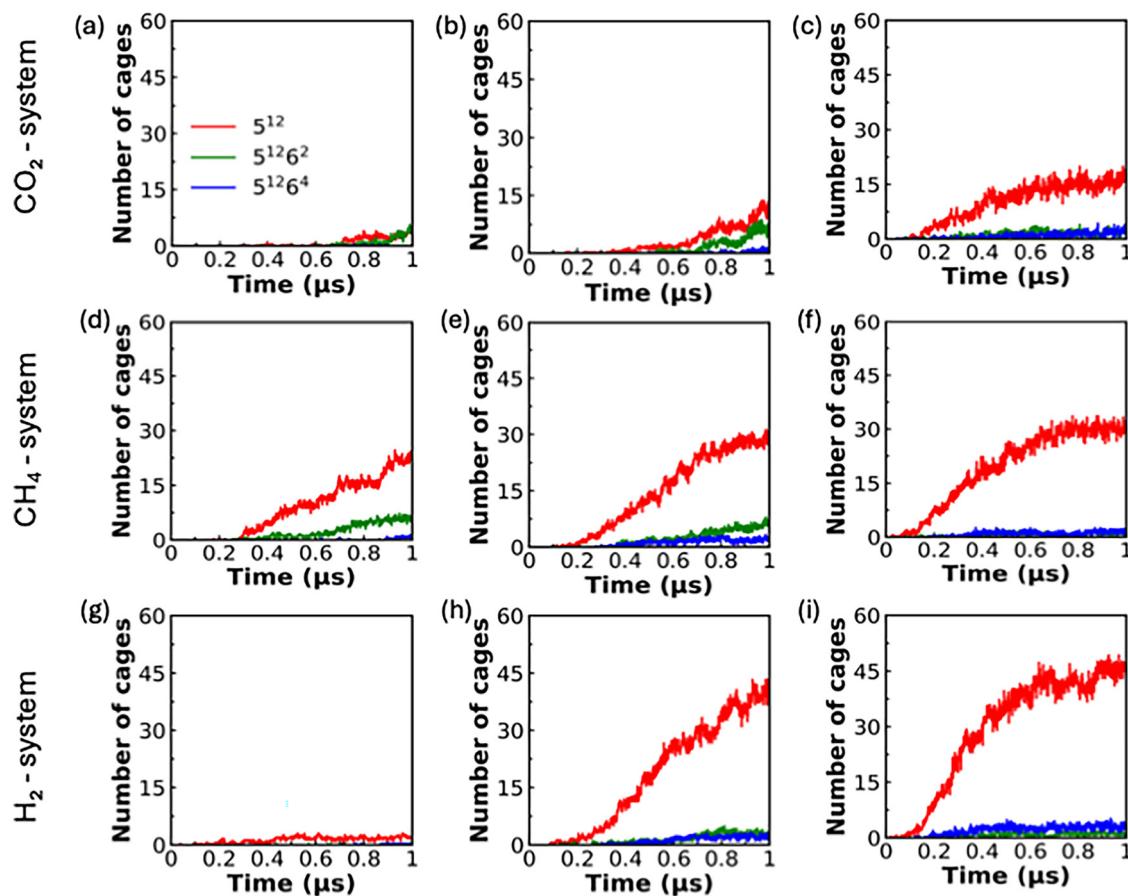


Fig. 4 Time evolution of the number of hydrate cages –  $5^{12}$ ,  $5^{12}6^2$ , and  $5^{12}6^4$  – formed in (a)–(c) the  $\text{CO}_2$  system, (d)–(f) the  $\text{CH}_4$  system, and (g)–(i) the  $\text{H}_2$  system at THF concentrations of 0% (left panels), 1.42% (middle panels), and 5.56% (right panels).

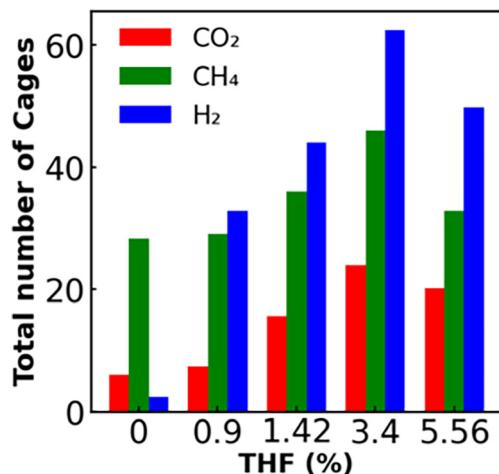


Fig. 5 The total average number of cages ( $5^{12}$ ,  $5^{12}6^2$ , and  $5^{12}6^4$ ) for the last 100 ns of the simulation for all the systems for different percentages of THF.

formation of amorphous hydrate phases during the nucleation and growth process.

Finally, we evaluate the number of gas molecules in the gas hydrates with different THF concentrations to reveal the gas uptake kinetics of  $\text{CO}_2$ ,  $\text{CH}_4$ , and  $\text{H}_2$  into clathrates. Fig. 6

shows the number of gas molecules in the hydrate at different concentrations of THF in solution for the system with  $\text{CO}_2$ ,  $\text{CH}_4$ , and  $\text{H}_2$  gases. The gas molecules trapped inside the cages are considered based on the center of mass distances between the cages and the gas molecules being less than 0.2 nm.<sup>62</sup> The results indicate that the number of gas molecules encapsulated within the hydrate cages increases with rising THF concentration during the early stages of gas hydrate formation. Specifically, gas uptake continues to increase up to a THF concentration of 3.4%. However, beyond this concentration, a noticeable decrease in  $\text{CO}_2$  occupancy within the hydrate cages is observed during the growth stage of hydrate formation. Additionally, our results reveal that, in the presence of THF, the overall gas uptake follows the order:  $\text{H}_2 > \text{CH}_4 > \text{CO}_2$ . These findings suggest that the optimal gas storage capacity is both gas-specific and dependent on the concentration of THF in the system.

Our results are consistent with experimental findings on  $\text{CO}_2$  gas hydrate formation from flue gas in the presence of THF, where the induction time decreases and gas uptake increases as the THF concentration increases from 1 mol% to 1.5 mol% in the solution.<sup>63</sup> Furthermore, our findings align with previous simulation studies, which demonstrate that the presence of THF significantly accelerates the rate of  $\text{CO}_2$



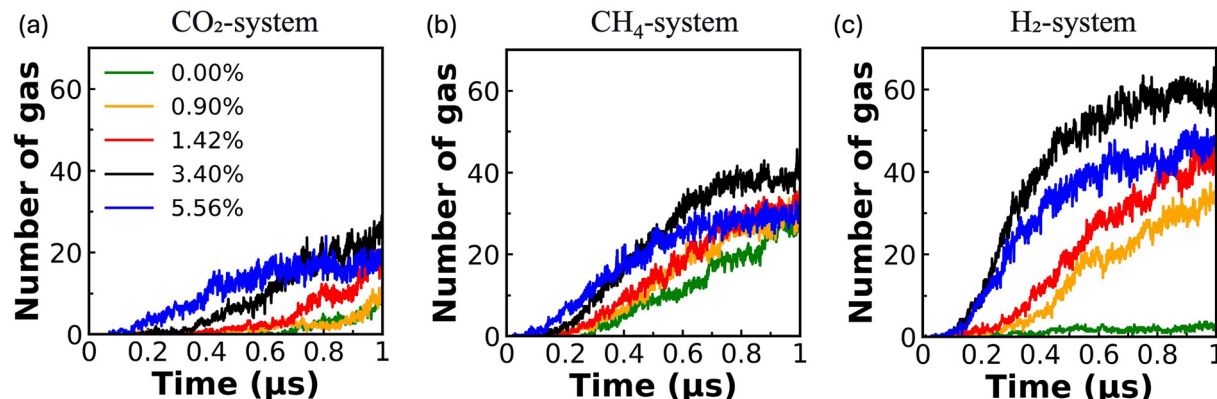


Fig. 6 The number of gas molecules encapsulated within the hydrate cages as a function of time at different THF concentrations for (a) the  $\text{CO}_2$  system, (b) the  $\text{CH}_4$  system, and (c) the  $\text{H}_2$  system.

hydrate formation compared to systems without THF.<sup>64,65</sup> It has also been reported that the storage stability and gas uptake capacity of THF- $\text{CH}_4$  hydrates are strongly influenced by process conditions. For  $\text{H}_2$  hydrate formation, no hydrate structures are observed in the absence of THF within the simulation timeframe, supporting the notion that THF stabilizes  $\text{H}_2$  clathrate hydrates by occupying large water cages.<sup>66,67</sup> Overall, the gas uptake and growth behavior of  $\text{CO}_2$ ,  $\text{CH}_4$ , and  $\text{H}_2$  hydrates in the presence of THF observed in this study are in good agreement with previously reported trends from both simulation and experimental investigations.

## 4. Conclusions

This study provides a comprehensive molecular-level understanding of the formation and stabilization mechanisms of  $\text{CO}_2$ ,  $\text{CH}_4$ , and  $\text{H}_2$  gas hydrates in the presence of THF using extensive MD simulations. By systematically varying THF concentrations, we elucidate how THF acts as a thermodynamic promoter, significantly influencing the nucleation, growth, and structural characteristics of gas hydrates. THF concentration above 1.42% markedly accelerates the nucleation of gas hydrates, with  $\text{CO}_2$  hydrates nucleating fastest, followed by  $\text{H}_2$  and  $\text{CH}_4$ . However, at higher THF concentrations,  $\text{H}_2$  hydrates exhibit the highest growth rate, as indicated by the  $F_4$  order parameter. The presence of THF increases the total number of hydrate cages, particularly up to a concentration of 3.4%, after which the effect plateaus for  $\text{CO}_2$  and  $\text{H}_2$  hydrates but leads to a decrease in cage formation for  $\text{CH}_4$  hydrates at even higher THF content. The initial nucleation predominantly involves the formation of small  $5^{12}$  cages, while larger  $5^{12}6^2$  and  $5^{12}6^4$  cages emerge during the growth phase, with their abundance and distribution being sensitive to both the gas type and THF concentration. Gas uptake analysis demonstrates that the number of guest molecules encapsulated within hydrate cages increases with THF concentration up to an optimal point, beyond which the effect varies by gas type. At higher THF concentrations,  $\text{H}_2$  shows the greatest uptake, followed by  $\text{CH}_4$  and  $\text{CO}_2$ , highlighting the tunable nature of gas storage capacity via THF concentration. Collectively, these insights advance our

understanding of the molecular dynamics governing gas hydrate nucleation and growth in mixed systems. The results underscore the important role of THF as a promoter, not only in modulating hydrate phase behavior and cage architecture but also in optimizing gas storage and sequestration strategies. The work will have fundamental implications in designing efficient gas hydrate-based technologies for energy storage, transportation, and environmental applications

## Conflicts of interest

There are no conflicts to declare.

## Data availability

The data supporting this article are available upon reasonable request from the corresponding authors.

## Acknowledgements

The work uses HPCE Aqua IIT Madras computational facility. This work is made possible by financial support from the SERB, DST, Govt of India through a core research grant (CRG/2022/006926).

## References

1. J. Carroll, *Natural Gas Hydrates: A Guide for Engineers*, Gulf Professional Publishing, 2020.
2. C. A. Koh, E. D. Sloan, A. K. Sum and D. T. Wu, Fundamentals and Applications of Gas Hydrates, *Annu. Rev. Chem. Biomol. Eng.*, 2011, **2**, 237–257.
3. K. A. Kvenvolden, Gas hydrates—geological perspective and global change, *Rev. Geophys.*, 1993, **31**, 173–187.
4. E. D. Sloan, Fundamental principles and applications of natural gas hydrates, *Nature*, 2003, **426**, 353–359.
5. M. D. Max, *Natural Gas Hydrate in Oceanic and Permafrost Environments*, Springer Science & Business Media, 2003.



6 L. Liu, Z. Sun, L. Zhang, N. Wu, Q. Yichao, Z. Jiang, W. Geng, H. Cao, X. Zhang, B. Zhai, C. Xu, Z. Shen and Y. Jia, Progress in Global Gas Hydrate Development and Production as a New Energy Resource, *Acta Geol. Sin. – Engl. Ed.*, 2019, **93**, 731–755.

7 Z. Xia, Q. Zhao, Z. Chen, X. Li, Y. Zhang, C. Xu and K. Yan, Review of methods and applications for promoting gas hydrate formation process, *J. Nat. Gas Sci. Eng.*, 2022, **101**, 104528.

8 P. Linga, R. Kumar, J. D. Lee, J. Ripmeester and P. Englezos, A new apparatus to enhance the rate of gas hydrate formation: Application to capture of carbon dioxide, *Int. J. Greenh. Gas Control*, 2010, **4**, 630–637.

9 E. D. Sloan Jr., Natural Gas Hydrates, *J. Pet. Technol.*, 1991, **43**, 1414–1417.

10 P. Englezos, Clathrate hydrates, *Ind. Eng. Chem. Res.*, 1993, **32**, 1251–1274.

11 M. T. Kirchner, R. Boese, W. E. Billups and L. R. Norman, Gas Hydrate Single-Crystal Structure Analyses, *J. Am. Chem. Soc.*, 2004, **126**, 9407–9412.

12 A. Khan, Stabilization of Hydrate Structure H by N<sub>2</sub> and CH<sub>4</sub> Molecules in 435663 and 512 Cavities, and Fused Structure Formation with 51268 Cage: A Theoretical Study, *J. Phys. Chem. A*, 2001, **105**, 7429–7434.

13 Y. F. Makogon, S. A. Holditch and T. Y. Makogon, Natural gas-hydrates—A potential energy source for the 21st Century, *J. Pet. Sci. Eng.*, 2007, **56**, 14–31.

14 J. F. Gabitto and C. Tsouris, Physical Properties of Gas Hydrates: A Review, *J. Thermodyn.*, 2010, 271291.

15 R. Kumar, P. Englezos, I. Moudrakovski and J. A. Ripmeester, Structure and composition of CO<sub>2</sub>/H<sub>2</sub> and CO<sub>2</sub>/H<sub>2</sub>/C<sub>3</sub>H<sub>8</sub> hydrate in relation to simultaneous CO<sub>2</sub> capture and H<sub>2</sub> production, *AIChE J.*, 2009, **55**, 1584–1594.

16 C. P. Ribeiro and P. L. C. Lage, Modelling of hydrate formation kinetics: State-of-the-art and future directions, *Chem. Eng. Sci.*, 2008, **63**, 2007–2034.

17 A. Kumar, O. S. Kushwaha, P. Rangsuvigit, P. Linga and R. Kumar, Effect of additives on formation and decomposition kinetics of methane clathrate hydrates: Application in energy storage and transportation, *Can. J. Chem. Eng.*, 2016, **94**, 2160–2167.

18 D. Mech, P. Gupta and J. S. Sangwai, Kinetics of methane hydrate formation in an aqueous solution of thermodynamic promoters (THF and TBAB) with and without kinetic promoter (SDS), *J. Nat. Gas Sci. Eng.*, 2016, **35**, 1519–1534.

19 E. Chaturvedi, S. Laik and A. Mandal, A comprehensive review of the effect of different kinetic promoters on methane hydrate formation, *Chin. J. Chem. Eng.*, 2021, **32**, 1–16.

20 A. A. A. Majid, J. Worley and C. A. Koh, Thermodynamic and Kinetic Promoters for Gas Hydrate Technological Applications, *Energy Fuels*, 2021, **35**, 19288–19301.

21 B. ZareNezhad, M. Mottahedin and F. Varaminian, Effects of process variables on the initial gas hydrate formation rate: The case of ethane hydrate formation in the absence or presence of SDS kinetic promoter, *J. Mol. Liq.*, 2014, **198**, 57–62.

22 A. Phan, H. Schlösser and A. Striolo, Molecular mechanisms by which tetrahydrofuran affects CO<sub>2</sub> hydrate Growth: Implications for carbon storage, *Chem. Eng. J.*, 2021, **418**, 129423.

23 N. Daraboina and N. von Solms, The Combined Effect of Thermodynamic Promoters Tetrahydrofuran and Cyclopentane on the Kinetics of Flue Gas Hydrate Formation, *J. Chem. Eng. Data*, 2015, **60**, 247–251.

24 Q. Nasir, H. Suleman and Y. A. Elsheikh, A review on the role and impact of various additives as promoters/inhibitors for gas hydrate formation, *J. Nat. Gas Sci. Eng.*, 2020, **76**, 103211.

25 Y.-J. Lee, T. Kawamura, Y. Yamamoto and J.-H. Yoon, Phase Equilibrium Studies of Tetrahydrofuran (THF) + CH<sub>4</sub>, THF + CO<sub>2</sub>, CH<sub>4</sub> + CO<sub>2</sub>, and THF + CO<sub>2</sub> + CH<sub>4</sub> Hydrates, *J. Chem. Eng. Data*, 2012, **57**, 3543–3548.

26 H. Wang, Q. Wu and B. Zhang, Influence of THF and THF/SDS on the Kinetics of CO<sub>2</sub> Hydrate Formation Under Stirring, *Front. Energy Res.*, 2021, **9**, 633929.

27 A. Phan, H. Schlösser and A. Striolo, Molecular mechanisms by which tetrahydrofuran affects CO<sub>2</sub> hydrate Growth: Implications for carbon storage, *Chem. Eng. J.*, 2021, **418**, 129423.

28 A. Kumar, N. Daraboina, R. Kumar and P. Linga, Experimental Investigation To Elucidate Why Tetrahydrofuran Rapidly Promotes Methane Hydrate Formation Kinetics: Applicable to Energy Storage, *J. Phys. Chem. C*, 2016, **120**, 29062–29068.

29 B.-B. Ge, D.-L. Zhong, Y.-Y. Lu and X.-Y. Li, Investigation of Tetrahydrofuran-CH<sub>4</sub> Hydrate Formation in Unstirred Conditions from a Different Perspective: Application to Solidified Natural Gas Storage, *Energy Fuels*, 2023, **37**, 15647–15656.

30 T. A. Strobel, C. A. Koh and E. D. Sloan, Thermodynamic predictions of various tetrahydrofuran and hydrogen clathrate hydrates, *Fluid Phase Equilib.*, 2009, **280**, 61–67.

31 M. Khurana, H. P. Veluswamy, N. Daraboina and P. Linga, Thermodynamic and kinetic modelling of mixed CH<sub>4</sub>-THF hydrate for methane storage application, *Chem. Eng. J.*, 2019, **370**, 760–771.

32 L. Jiang, Z. Cheng, S. Li, N. Xu, H. Xu, J. Zhao, Y. Liu, M. Yu and Y. Song, High-efficiency gas storage via methane-tetrahydrofuran hydrate formation: Insights from hydrate structure and morphological analyses, *Fuel*, 2022, **311**, 122494.

33 B. Mahant, M. T. J. Barwood, D. J. Zhu, C. Li, R. Kumar and E. F. May, Phase Equilibria and Nucleation Rates of Mixed Methane-Tetrahydrofuran Gas Hydrates for Energy Storage, *Energy Fuels*, 2025, **39**, 3859–3867.

34 S. Hashimoto, T. Sugahara, H. Sato and K. Ohgaki, Thermodynamic Stability of H<sub>2</sub> + Tetrahydrofuran Mixed Gas Hydrate in Nonstoichiometric Aqueous Solutions, *J. Chem. Eng. Data*, 2007, **52**, 517–520.

35 J. Zhang, Y. Li, Z. Yin, X. Y. Zheng and P. Linga, How THF Tunes the Kinetics of H<sub>2</sub>-THF Hydrates? A Kinetic Study with Morphology and Calorimetric Analysis, *Ind. Eng. Chem. Res.*, 2023, **62**, 21918–21932.

36 J. Cai, Y.-Q. Tao, N. Von Solms, C.-G. Xu, Z.-Y. Chen and X.-S. Li, Experimental studies on hydrogen hydrate with tetrahydrofuran by differential scanning calorimeter and in-situ Raman, *Appl. Energy*, 2019, **243**, 1–9.



37 D. W. Kang, W. Lee, Y.-H. Ahn and J. W. Lee, Exploring tuning phenomena of THF-H<sub>2</sub> hydrates via molecular dynamics simulations, *J. Mol. Liq.*, 2022, **349**, 118490.

38 J. Cai, Y.-Q. Tao, N. Von Solms, C.-G. Xu, Z.-Y. Chen and X.-S. Li, Experimental studies on hydrogen hydrate with tetrahydrofuran by differential scanning calorimeter and in-situ Raman, *Appl. Energy*, 2019, **243**, 1–9.

39 V. Hande, N. Choudhary, S. Chakrabarty and R. Kumar, Morphology and dynamics of self-assembled structures in mixed surfactant systems (SDS + CAPB) in the context of methane hydrate growth, *J. Mol. Liq.*, 2020, **319**, 114296.

40 P. Kanani, K. Ganesh Reddy, M. Adil and A. K. Metya, Impact of antifreeze and promoter on clathrate hydrate nucleation and growth, *J. Mol. Liq.*, 2025, **424**, 127118.

41 J. L. F. Abascal, E. Sanz, R. García Fernández and C. Vega, A potential model for the study of ices and amorphous water: TIP4P/Ice, *J. Chem. Phys.*, 2005, **122**, 234511.

42 J. G. Harris and K. H. Yung, Carbon Dioxide's Liquid-Vapor Coexistence Curve And Critical Properties as Predicted by a Simple Molecular Model, *J. Phys. Chem.*, 1995, **99**, 12021–12024.

43 W. L. Jorgensen, D. S. Maxwell and J. Tirado-Rives, Development and Testing of the OPLS All-Atom Force Field on Conformational Energetics and Properties of Organic Liquids, *J. Am. Chem. Soc.*, 1996, **118**, 11225–11236.

44 V. Buch, Path integral simulations of mixed para-D2 and ortho-D2 clusters: The orientational effects, *J. Chem. Phys.*, 1994, **100**, 7610–7629.

45 P. Procacci, PrimaDORAC: A Free Web Interface for the Assignment of Partial Charges, Chemical Topology, and Bonded Parameters in Organic or Drug Molecules, *J. Chem. Inf. Model.*, 2017, **57**, 1240–1245.

46 B. Hess, H. Bekker, H. J. C. Berendsen and J. G. E. M. Fraaije, LINCS: A linear constraint solver for molecular simulations, *J. Comput. Chem.*, 1997, **18**, 1463–1472.

47 T. Darden, D. York and L. Pedersen, Particle mesh Ewald: An N-log(N) method for Ewald sums in large systems, *J. Chem. Phys.*, 1993, **98**, 10089–10092.

48 A. Iserles, Generalized Leapfrog Methods, *IMA J. Numer. Anal.*, 1986, **6**, 381–392.

49 J. C. Meza, Steepest descent, *WIREs Comput. Stat.*, 2010, **2**, 719–722.

50 H. J. C. Berendsen, J. P. M. Postma, W. F. van Gunsteren, A. DiNola and J. R. Haak, Molecular dynamics with coupling to an external bath, *J. Chem. Phys.*, 1984, **81**, 3684–3690.

51 W. G. Hoover, Canonical dynamics: Equilibrium phase-space distributions, *Phys. Rev. A*, 1985, **31**, 1695–1697.

52 S. Nosé, A molecular dynamics method for simulations in the canonical ensemble, *Mol. Phys.*, 1984, **52**, 255–268.

53 M. Parrinello and A. Rahman, Crystal Structure and Pair Potentials: A Molecular-Dynamics Study, *Phys. Rev. Lett.*, 1980, **45**, 1196–1199.

54 B. Hess, C. Kutzner, D. van der Spoel and E. Lindahl, GROMACS 4: Algorithms for Highly Efficient, Load-Balanced, and Scalable Molecular Simulation, *J. Chem. Theory Comput.*, 2008, **4**, 435–447.

55 M. R. Walsh, C. A. Koh, E. D. Sloan, A. K. Sum and D. T. Wu, Microsecond Simulations of Spontaneous Methane Hydrate Nucleation and Growth, *Science*, 2009, **326**, 1095–1098.

56 S. A. Bagherzadeh, S. Alavi, J. Ripmeester and P. Englezos, Formation of methane nano-bubbles during hydrate decomposition and their effect on hydrate growth, *J. Chem. Phys.*, 2015, **142**, 214701.

57 Z. He, K. M. Gupta, P. Linga and J. Jiang, Molecular Insights into the Nucleation and Growth of CH<sub>4</sub> and CO<sub>2</sub> Mixed Hydrates from Microsecond Simulations, *J. Phys. Chem. C*, 2016, **120**, 25225–25236.

58 M. Pan, P. Naeiji and N. J. English, Fate of Nanobubbles Generated from CO<sub>2</sub>-Hydrate Dissociation: Coexistence with Nanodroplets—A Combined Investigation from Experiment and Molecular Dynamics Simulations, *Small Struct.*, 2024, **5**, 2400080.

59 K. Inkong, K. Jeemuang, S. Kulprathipanja and P. Rangsuvigit, Investigation of Hydrate Formation and Stability of Mixed Methane-THF Hydrates: Effects of Tetrahydrofuran Concentration, *J. Oleo Sci.*, 2024, **73**, 1159–1168.

60 P. Babu, H. W. N. Ong and P. Linga, A systematic kinetic study to evaluate the effect of tetrahydrofuran on the clathrate process for pre-combustion capture of carbon dioxide, *Energy*, 2016, **94**, 431–442.

61 Z.-Y. Li, Z.-M. Xia, Z.-Y. Chen, X.-S. Li, C.-G. Xu and R. Yan, The plateau effects and crystal transition study in Tetrahydrofuran (THF)/CO<sub>2</sub>/H<sub>2</sub> hydrate formation processes, *Appl. Energy*, 2019, **238**, 195–201.

62 F. Mahmoudinobar and C. L. Dias, GRADE: A code to determine clathrate hydrate structures, *Comput. Phys. Commun.*, 2019, **244**, 385–391.

63 P. Linga, R. Kumar, J. D. Lee, J. Ripmeester and P. Englezos, A new apparatus to enhance the rate of gas hydrate formation: Application to capture of carbon dioxide, *Int. J. Greenh. Gas Control*, 2010, **4**, 630–637.

64 X. Yang, S. Du, Y. Hao and J. Xu, Molecular dynamics simulation of promoting nucleation of CO<sub>2</sub> hydrate by ethylene oxide and tetrahydrofuran, *IOP Conf. Ser. Earth Environ. Sci.*, 2021, **675**, 012183.

65 P. Kanani, K. Ganesh Reddy, M. Adil and A. K. Metya, Impact of antifreeze and promoter on clathrate hydrate nucleation and growth, *J. Mol. Liq.*, 2025, **424**, 127118.

66 L. J. Florusse, C. J. Peters, J. Schoonman, K. C. Hester, C. A. Koh, S. F. Dec, K. N. Marsh and E. D. Sloan, Stable Low-Pressure Hydrogen Clusters Stored in a Binary Clathrate Hydrate, *Science*, 2004, **306**, 469–471.

67 H. Lee, J. Lee, D. Y. Kim, J. Park, Y.-T. Seo, H. Zeng, I. L. Moudrakovski, C. I. Ratcliffe and J. A. Ripmeester, Tuning clathrate hydrates for hydrogen storage, *Nature*, 2005, **434**, 743–746.

